Effect of curing conditions on the pore solution and carbonation resistance of alkali-activated fly ash and slag pastes

Nedeljković, Marija; Ghiassi, Bahman; van der Laan, Sieger; Li, Zhenming; Ye, Guang

DOI
10.1016/j.cemconres.2018.11.011

Publication date
2019

Document Version
Accepted author manuscript

Published in
Cement and Concrete Research

Citation (APA)
Nedeljković, M., Ghiassi, B., van der Laan, S., Li, Z., & Ye, G. (2019). Effect of curing conditions on the pore solution and carbonation resistance of alkali-activated fly ash and slag pastes. *Cement and Concrete Research*, *116*, 146-158. https://doi.org/10.1016/j.cemconres.2018.11.011

Effect of curing conditions on the pore solution and carbonation resistance of alkali-activated fly ash and slag pastes

Marija Nedeljković[a*], Bahman Ghiassi[a,b], Sieger van der Laan[c], Zhenming Li[a], Guang Ye[a,d]

[a]Microlab, Faculty of Civil Engineering and Geosciences, Delft University of Technology, Stevinweg 1, 2628 CN Delft, The Netherlands

[b]Centre for Structural Engineering and Informatics, Department of Civil Engineering, The University of Nottingham, UK

[c]Tata Steel, R&D, P.O. Box 10.000, 1970 CA IJmuiden, The Netherlands

[d] Magnel Laboratory for Concrete Research, Department of Structural Engineering, Ghent University Technologiepark-Zwijnaarde 904 B-9052, Ghent (Zwijnaarde), Belgium

e-mail: M.Nedeljkovic@tudelft.nl
bahman.ghiassi@nottingham.ac.uk
sieger.van-der-laan@tatasteel.com
Z.Li-2@tudelft.nl
G.Ye@tudelft.nl

[*] Corresponding author
Tel: +31 (0)15 278 4554

ABSTRACT

The effect of curing conditions (sealed and unsealed) on the pore solution composition and carbonation resistance of different binary alkali-activated fly ash (FA) and ground granulated blast furnace slag (GBFS) pastes is investigated in this study. The studied mixtures were with FA/GBFS ratios of 100:0, 70:30; 50:50, 30:70, 0:100. Ordinary Portland cement (OPC) and Cement III/B (70 wt.% of GBFS and 30 wt.% OPC) pastes with the same precursor content were also studied to provide a baseline for comparison. Accelerated carbonation conditions (1% (v/v) CO_2, 60% RH for 500 days) were considered for evaluating the carbonation resistance of the pastes.

The results show a substantial lower [Na^+] in the pore solution of the unsealed cured samples compared to the sealed cured samples. It is also found that unsealed curing of the samples leads to a faster carbonation rate. Additionally, it is observed that the carbonation rate decreases with increasing GBFS content independent of the curing conditions. The potential risks with respect to carbonation of the pore solution are also identified and discussed.

Keywords: Alkali-activated fly ash/slag; Curing condition; Pore solution; Carbonation.

1. Introduction

Carbonation is one of the most harmful degradation processes that can significantly affect the performance of reinforced Portland cement (OPC)-based concrete structures [1] and for this reason, has been the subject of many studies in the literature [2-6]. Understanding this degradation mechanism in alkali-activated materials (AAMs) that has received extensive attention as a sustainable construction material is therefore of critical importance for their standardization and use in practice [7].

In conventional OPC-based concrete, carbonation is the result of chemical reaction between carbonic acid and cement hydration products that leads to precipitation of carbonation products and decrease in the pH of the pore solution [8]. Carbonic acid is formed in the pore solution by dissolution of gaseous CO_2 that diffuses from the environment into the porous structure of the concrete. Carbonation, which is controlled by both diffusion and chemical reaction, is dependent on several factors including relative humidity, tortuosity of the paste, concentration of CO_2 in the environment and chemistry of the binder [9, 10].

Although the carbonation mechanism in AAMs is not yet fully understood, it is expected to be different from that of OPC-based concrete. The fundamental differences in the constituting phases and the physical structure of AAMs in comparison to OPC-based

materials is the main reason for such an expectation [11]. While the main reaction products in OPC-based materials are $Ca(OH)_2$ and C-S-H, different types of alkaline gel are formed in AAMs, such as sodium aluminosilicate hydrate (N-A-S-H), calcium aluminosilicate hydrate (C-A-S-H) and calcium sodium aluminosilicate hydrate (C-N-A-S-H) [12-14]. AAMs in contrast to OPC-based concrete, do not contain $Ca(OH)_2$ [15]. The absence of $Ca(OH)_2$, that acts as the main buffering compound in OPC-based concrete, leads to faster decalcification of C-A-S-H/C-N-A-S-H gels and may account for the faster carbonation process in AAMs [16, 17].

It seems that carbonation in AAMs occurs in two main steps [18]: (1) Carbonation of the pore solution leading to reduction of pH and precipitation of Na-rich carbonates; (2) decalcification of Ca-rich phases and secondary products present in the system. This suggests that the carbonation resistance of AAMs is not only a function of their binding capacity (or the reactive CaO content) as reported for cement based materials [10], but also of the Na_2O content consumed during the reaction of the precursors (e.g. FA and GBFS) [19]. Furthermore, the carbonation mechanism is strongly influenced by the type of the precursor (FA, GBFS or metakaoline) [20-22], the nature and dosage of the alkaline activator used [23], the exposure conditions [24] and the curing conditions, amongst others. While several recent studies can be found in the literature investigating the effects of these parameters on the carbonation resitance of AAMs, the role of curing conditions on the potential Na^+ loss and carbonation resistance has not been reported yet.

The use of highly alkaline activators for reactions of the FA and GBFS provides a high $[Na^+]$ leading to high pH levels in the pore solution of noncarbonated AAMs. It has been shown that this ensures existence of sufficiently high $[Na^+]$ after natural and accelerated carbonation in alkali-activated systems to prevent corrosion of reinforcement [19]. However,

it is not clear whether the succeptibility of AAMs to loss of Na^+ ions prior to (or during) the carbonation process can lead to significant decrease of pH or not [25-27].

The aim of this paper is to address these questions by investigating the effect of curing conditions on the pore solution chemistry and carbonation resistance of alkali-activated FA/GBFS pastes. Special attention is given to the Na^+ loss in sealed and unsealed cured specimens. Five mixtures with different FA/GBFS ratio are investigated. OPC (CEM I) and CEM III/B pastes are considered to provide a baseline and to perform comparisons with the studied alkali activated pastes.

2. Materials and methods

2.1 Materials and sample preparation

FA was supplied by VLIEGASUNIE BV and GBFS was supplied by ORCEM (the Netherlands). CEM I 42.5 N and CEM III/B 42.5 N in compliance with Dutch standard (NEN-EN 197-1:2011 en) were used as references. The chemical composition of raw materials was determined with X-ray Fluorescence (XRF) (Table 1). XRF measurements were done using Panalytical AXIOS Max Advanced XRF spectrometer. XRF analysis of raw materials was performed with fused beads and lithium tetraborate/methaborate as a flux. XRF bead analysis is not suitable for the analysis of sulfur. Therefore, sulphur (S) was determined using Eltra Sulphur analyzer. Loss on ignition (LOI) was determined by LECO Thermographic Analyser (TGA701). The negative LOI for GBFS (Table 1) was related to the oxidation of sulfur rich species in the GBFS. It should be noted that the LOI was not corrected in the XRF measurements. The average particle size of GBFS, d_{50}, was 19 μm, while for FA, d_{50} was 21 μm, as measured by the laser diffraction analyser.

Table 1

Chemical compositions of FA, GBFS, CEM I (42.5 N), CEM III-B measured with XRF [%].

	SiO_2	Al_2O_3	CaO	MgO	Fe_2O_3	S	Na_2O	K_2O	TiO_2	P_2O_5	LOI
FA	56.8	23.8	4.8	1.5	7.2	0.3	0.8	1.6	1.2	0.5	1.2
GBFS	35.5	13.5	39.8	8.0	0.6	1.0	0.4	0.5	1.0	0.0	-1.3
CEM I	19.6	4.8	62.2	1.8	3.0	1.4	0.4	0.6	0.3	0.2	2.8
CEM III-B	30.0	11.0	45.0	7.0	1.3	1.9	0.4	0.5	0.9	0.6	0.1

Alkaline activator was prepared by mixing anhydrous pellets of sodium hydroxide with deionized water and commercial sodium silicate solution (27.5 wt.% SiO_2, 8.25 wt.% Na_2O). After mixing, activator liquid was kept under the laboratory conditions with the temperature around 20°C to cool down for 24 h prior to the paste mixing. The activator Na_2O concentration was 4.8 wt.% with respect to the mass of precursor (FA + GBFS). For each paste, the activator liquid to binder mass ratio was 0.5. The pastes were produced with the following FA/GBFS ratios of 100:0, 70:30, 50:50, 30:70, 0:100 wt.%, named S0, S30, S50, S70, S100, respectively (Table 2). Cement pastes were made with water-to-binder ratio 0.5.

Table 2

Mixture design for pastes with respect to 100 g of the binder.

Mixture	FA[a]	GBFS[b]	OPC[c]	m(Na_2O)/ m(binder)	SiO_2/ Na_2O	water/ binder	activator liquid/ binder	Curing regime
S0	100	0	0	4.80	1.45	0.38	0.50	Unsealed/ Sealed
S30	70	30						
S50	50	50						
S70	30	70						
S100	0	100						
CEM III-B	0	70	30	-	-	0.50		
CEM I	0	0	100					

[a, b, c]weight percentage with respect to raw material (FA, GBFS, OPC) content (wt. %).

The precursors were dry-mixed for 2 minutes and then mixed with the activator. The pastes were cast in two types of cylindric polyethylene jars, (A) with 35 mm diameter and 70

mm height, and (B) with 54 mm diameter and 100 mm height and vibrated for 15-30 s on a vibrating table. The samples denoted as (A) were used for RH measurements pore solution extraction and alkali loss measurements, while samples (B) were used for mass loss, carbonation depth and pH measurements. The samples were stored in the closed jars (A, B) for 24 h after casting. For unsealed cured conditions, samples were removed from the jars and afterwards cured in a fog room at room temperature and a relative humidity (RH) of ~99% RH (the atmosphere was normal air with 400 ppm of CO_2 and the air was internally circulated, however, when opening the curing room, air with CO_2 is expected to enter the fog room) for 28 days. For sealed samples, these were kept in the jars in the curing room where unsealed samples were also cured.

2.2 Test programme

An overview is shown in the Fig. 1 of the test programme followed to investigate the effect of curing conditions and accelerated carbonation on the alkali-activated FA/GBFS pastes. First mass loss, internal RH, pore solution composition and pH are studied both for curing under sealed and unsealed conditions. Additionally, alkali loss was monitored for unsealed cured samples during the first 28 days of curing. The sealed samples were unsealed after 28 days of curing when all the samples were placed in the laboratory conditions at 55-60% RH (0.04% v/v CO_2, 20°C) for additional 28 days (preconditioning of the samples prior to carbonation). This preconditioning was intended to equilibrate the internal RH of the samples with the environment before performing the accelerated carbonation tests. For unsealed samples, one set was left in the curing room for an additional 28 days, to provide insight into the further alkali loss after first 28 days of curing.

During carbonation exposure, the carbonation depth was monitored in both sealed and unsealed cured samples.

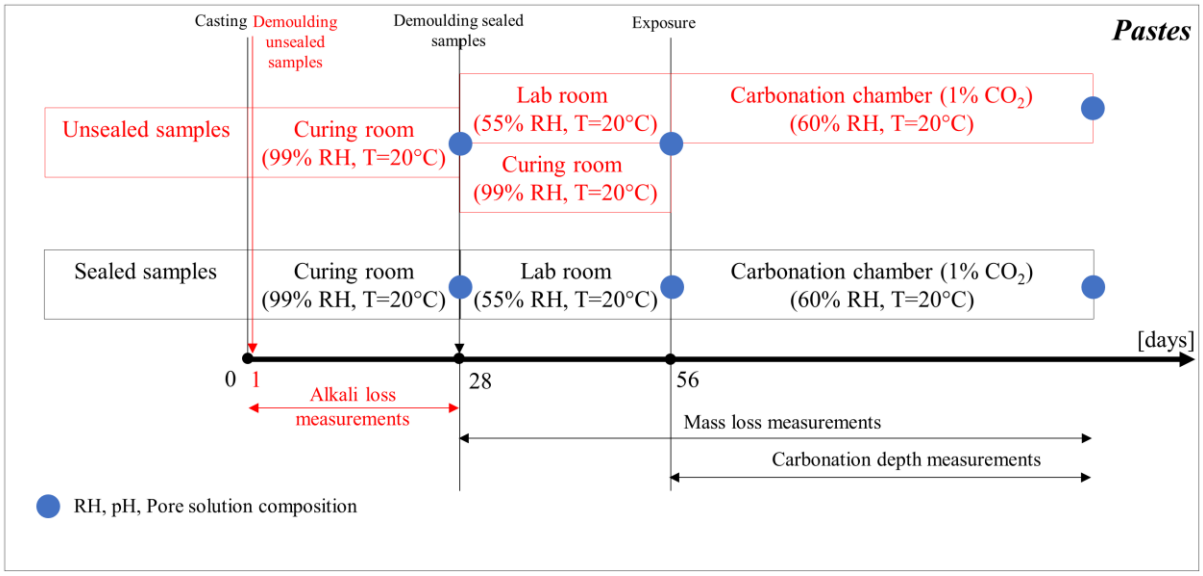

Fig. 1. Schematic representation of the test programme.

2.2.1 RH measurements

Free water in the pore structure of the pastes is critical for carbonation progress. In order to ensure that the internal relative humidity of the pastes is in equilibrium with RH of the carbonation chamber, the internal RH of the pastes was measured after 1 day (before demoulding of the samples), after 28 days of curing and after 28 days of preconditioning (a total of 56 days). The procedure for internal RH measurements follows Huang et al. [28]. The internal RH of bulk pastes (A) was measured by Rotronic HygroLab C1 equipped with two HC2-AW RH station probes with an accuracy of ±1 % RH. The RH probes were calibrated using saturated salt solutions with known constant RH in the range of 65-95%. The samples were cut in thin slices of less than 7 mm, so in the sample holder there were a few slices of one sample. The sample slices were then put in two plastic containers in the measuring chambers. Samples and atmosphere equilibrated in 3-5 hours. The measured RH represents the average of the internal RH and it is not related to RH of a specific depth of the samples.

2.2.2 Mass loss measurements

Mass loss measurements were used to assure that preconditioning period of 28 days is sufficient prior exposure of samples to accelerated carbonation. The mass loss of the sealed and unsealed pastes after 28 days of curing was monitored in the laboratory conditions (55% RH, 20 °C) until constant mass was reached. The mass of samples was measured since the samples were removed from the curing room. It was observed that at the age of 56 days the difference between two measurements was less than 0.01 g. Based on this observation, the samples were preconditioned for 28 days before carbonation exposure (curing of 28 days and preconditioning of 28 days), as indicated in Fig. 1. The evaporable water in the pastes was also determined (at specific periods) by measuring the weight loss per gram of the samples at 105ºC in an oven (Jouan oven Type E455 EL), until reaching a constant weight.

2.2.3 Pore solution composition and pH measurements

Procedure for pore solution extraction from alkali-activated FA/GBFS pastes is adopted from [29]. The pore solutions were pressed out from the pastes (type A sample size with 35 mm diameter and 70 mm height) with a high-pressure apparatus MacBen-type, with an oil-hydraulic end-load capacity of 5000 kN and a cylinder assembly with an inner diameter of 34 mm and a height of 115 mm fitting the size of the paste cylinders (A). Pressures of up to 750 MPa were used to extract the pore fluid. The fluid was extracted through a drain channel and collected in a syringe with almost no exposure to the atmosphere. Around 0.5 to 5 ml of pore solution could be collected for each sample depending on the type of the paste and the curing age. The pressed-out pore solutions were filtered using Whatman 41 filter paper and half of each solution was diluted using nitric acid (0.2 vol.%). Inductively coupled plasma optical emission spectrometry (ICP-OES) was used for chemical analysis of the pore solution

composition. Chemical analyses of diluted solutions were carried out with a Perkin Elmer Optima 5300 DV apparatus.

The pH was measured on the non-diluted solutions. The non-diluted solutions of the samples cured for 28 days and 56 days were left for measurement of [OH^-] by titration against HCl acid. While pore fluid extraction from the original samples was successful, direct extraction from carbonated samples was not possible due to both the low relative humidity used during the carbonation process and the small amount of sample material. Therefore, the pH measurements were carried out on simulated pore solutions similar to [30], by equilibrating 1 g of powdered paste (bulk pastes were crushed and ground into a powder) with 10 ml of de-ionized water during 15 minutes at ambient temperature while stirring with a magnetic bar. Subsequently, the pH of the suspension was measured by pH meter 827 Metrohm. The powders were obtained from the outer surface of the samples within a thickness of 1 mm. These simulated pore solutions were used as a substitute for pressed-out fluids to compare non-carbonated samples with 500 days curing (as reference) with samples carbonated for 500 days.

2.2.4 Alkali loss measurements

It was noticed from measurements of the pore solution composition that unsealed curing is associated with a leaching process induced by the RH of curing room in which mainly Na^+ loss from the paste body occurs. A common curing set-up was used for alkali loss measurements to confirm Na^+ loss. The test set-up is shown in Fig. 2. The specimens (sealed and unsealed) after 1 day of casting, were placed in the curing room with 99% RH and 20°C. Moisture condensed on the surface of the specimens was collected in plastic containers that were placed under the specimens. After 1, 4, 7, 21, 28 days, the liquid from the plastic containers was collected to analyse [Na^+] in the leached solutions. The collected liquid was

filtered using Whatman 41 filter paper. Afterwards, the liquid was diluted using nitric acid (0.2 vol.%). Chemical analyses of the diluted liquids were carried out with a Perkin Elmer Optima 5300 DV apparatus.

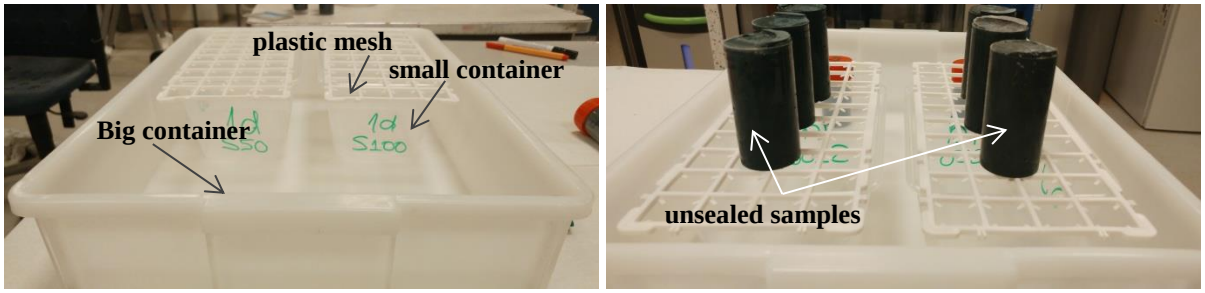

Fig. 2. Set up for alkali loss measurements.

2.2.5 Accelerated carbonation conditions and carbonation depth measurements

Accelerated carbonation started 56 days after curing and preconditioning, in a CO_2 atmosphere of 1% v/v at 60% RH and at 20°C. The CO_2 of 1% v/v was chosen since it was reported by Bernal et al. [20] that conducting accelerated carbonation using CO_2 concentrations beyond CO_2~1% v/v will not accurately replicate the carbonation mechanisms observed in service. The carbonation depth was measured with phenolphthalein, according to the standard EN 13295:2004. Carbonation depths of the cylindric pastes (B) were measured after 1, 7, 14, 28, 56, 90, 180, 270, 365, 500 days of CO_2 exposure. The cylinders were split and the fresh surface was sprayed with a 1 wt. % phenolphthalein solution (comprising 1 g of phenolphthalein in a solution of 70 ml ethanol and 30 ml demineralized water). The recorded carbonation depths are the average of measurements at 10 locations on the sample.

2.2.6 ESEM-EDX

Investigation of the morphology and element composition of the deposits found on the surface of the unsealed cured samples and in the small plastic containers (Fig. 2) was done

with the Philips-XL30-ESEM microscope, equipped with NSS.3.3. The deposit was collected from the sample surface with a brush, while the liquid drop of the deposit was collected from the small plastic container. For scanning electron microscope/energy-dispersive X-ray (SEM-EDX) analysis, deposits were placed onto carbon-coated sticky stubs and directly observed under the ESEM-BSE mode.

3. Results and discussions

3.1 Effect of the curing conditions

3.1.1 Mass loss and internal RH

The changes of the mass of the specimens with time are presented in Fig. 3 and Fig. 4. The total mass percentage of water loss in the pastes due to drying after 28 days storage in the laboratory conditions (55% RH and 20°C) is presented in Table 3. It proves that in all samples a fluid phase is present and that RH is not buffered solely by solid phases when starting carbonation.

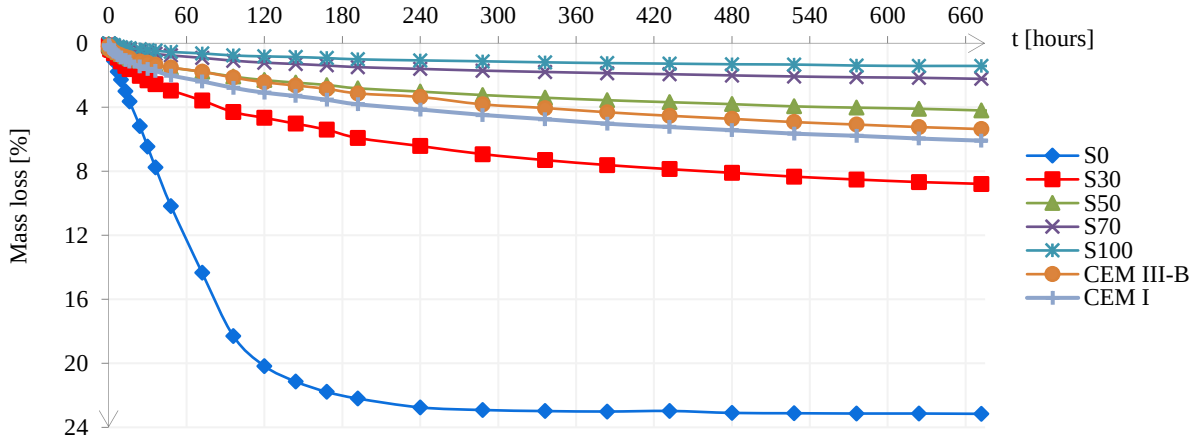

Fig. 3. Unsealed samples first 28 days; mass loss measured from 28 days.

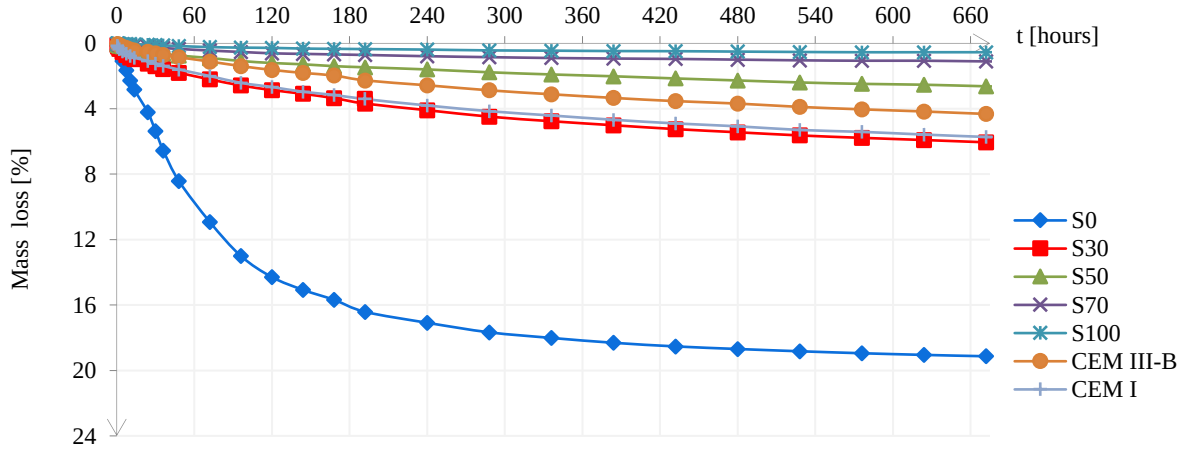

Fig. 4. Sealed samples first 28 days; mass loss measured from 28 days.

Table 3

Water loss (in mass percentage) and internal RH of the pastes*.

	Sample mass [g]		Water loss [wt.%]						Internal RH [%]				
	At age of 28 days		Stored in lab RH 55% conditions from age of 28 d to 56 d		Heating at 105°C (at 56d)		Total water loss		1d**	28d		56d	
	sealed	unsealed	sealed	unsealed	sealed	unsealed	sealed	unsealed	sealed	sealed	unsealed	sealed	unsealed
S0	349.5	359.8	19.13	23.15	5.05	3.08	24.18	26.23	> 95.00	> 95.00	> 95.00	64.1	64.3
S30	376.6	379.4	6.05	8.78	14.45	13.87	20.50	22.65	> 95.00	> 95.00	> 95.00	64.6	65.0
S50	382.0	381.7	2.63	4.20	16.90	17.00	19.53	21.20	91.88	90.30	94.00	64.1	65.0
S70	401.0	397.4	1.10	2.22	17.81	17.80	18.91	20.02	88.12	80.80	80.00	63.8	64.0
S100	413.0	413.9	0.55	1.42	16.73	17.12	17.28	18.54	87.07	71.50	73.00	62.3	62.0
CEM III/B	365.0	358.2	4.32	5.36	19.96	20.39	24.28	25.75	> 95.00	> 95.00	> 95.00	78.9	80.0
CEM I	353.0	342.9	5.72	6.08	22.00	22.10	27.72	28.18	> 95.00	> 95.00	> 95.00	70.4	73.0

*'Sealed' are the samples that were cured in sealed conditions first 28 days and then demoulded and exposed to lab conditions until 56 days. 'Unsealed' are the samples that were cured in 20 ºC, ~99 % RH conditions during the first 28 days and further exposed to lab conditions until 56 days.

**The 1d internal RH presents the time zero when the samples were removed from moulds to curing room (all samples were kept in moulds for 1 day before curing in the fog room). The RH of the activation solution (NaOH+WG) before mixing with raw FA and GBFS was 92.03%.

In general, the amount of evaporable water for the unsealed cured samples are higher compared to the sealed. The amount of evaporable water between conditions of 99% RH and 28 days curing and subsequent 55% RH exposure until 56 days is the highest in paste S0 and the lowest in paste S100. In alkali-activated FA materials, a much higher Na_2O concentration and curing temperatures (> 40°C) are required for a complete dissolution of FA [31]. In the present study, due to the low Na_2O concentration of the alkaline activator and the applied curing conditions (ambient temperature) paste S0 has a limited degree of reaction which is supported by the low strength development observed in [32]. This low reaction degree implies the existence of physical water in the pores as experimentally measured here, see Fig. 3 and Fig. 4. On the other hand, based on the measurements of the evaporable water content at 105°C, it can be seen that with increasing GBFS content more evaporable water is measured at 105°C, than at 55% RH. This suggests that GBFS-rich pastes have more chemically bound water than FA-rich pastes. Another effect that can be observed is that with increasing GBFS the total free water (sum of evaporated at 55% RH + mass loss at 105°C) decreases, implying that some water must become structurally bound in the samples equivalent to self-dessication.

The mechanisms affecting the transport of physical water in unsealed cured samples are illustrated in Fig. 5a. The loss of alkalis in the case of unsealed samples exposed to 99% RH is due to several counter-affecting phenomena (Fig.5b). The RH of the activation solution (NaOH+WG) before mixing with raw FA and GBFS was 92.03%, while the RH of the pastes S30, S50, S70 and S100 at 1 day (when 99% RH curing initiated) was 95.86%, 91.88%, 88.12%, 86.98%, respectively (see Table 3). This difference in the RH of the environment and the specimen, causes a capillary flow from the surface to the interior of the samples and therefore an inward movement of the ions (advection). Meanwhile, condensation of water on the surface of the samples leads to dilution of the ions at the surface compared to the interior of the specimens. This causes a diffusive movement of ions from the interior towards the

surface of the samples. There is, therefore, a clear competition between both phenomena. Based on the observed [Na^+] difference in the pore solution in sealed and unsealed curing conditions (see Table 4), the second mechanism is predominant in the studied samples. Both advection and diffusion are governed by the microstructure of the paste and, for that reason, the alkali loss is different between the studied alkali activated pastes (see Fig. 9).

On the other hand, when samples are moved from the curing room, subsequent drying of the surface causes efflorescence (see Fig. 5a, drying 28-56 days). The product of efflorescence is calcite as will be shown in Fig. 8a. Calcite was formed already in the curing room on the wet outer surface of the samples. In the high pH fluid, CO_2 will be present as CO_3^{2-} and together with Ca^{2+} it forms calcite. The calcium carbonate efflorescence is promoted even at smaller amounts of alkali dissolved in the aqueous film such as in cement based pastes [33], compared to alkali activated pastes.

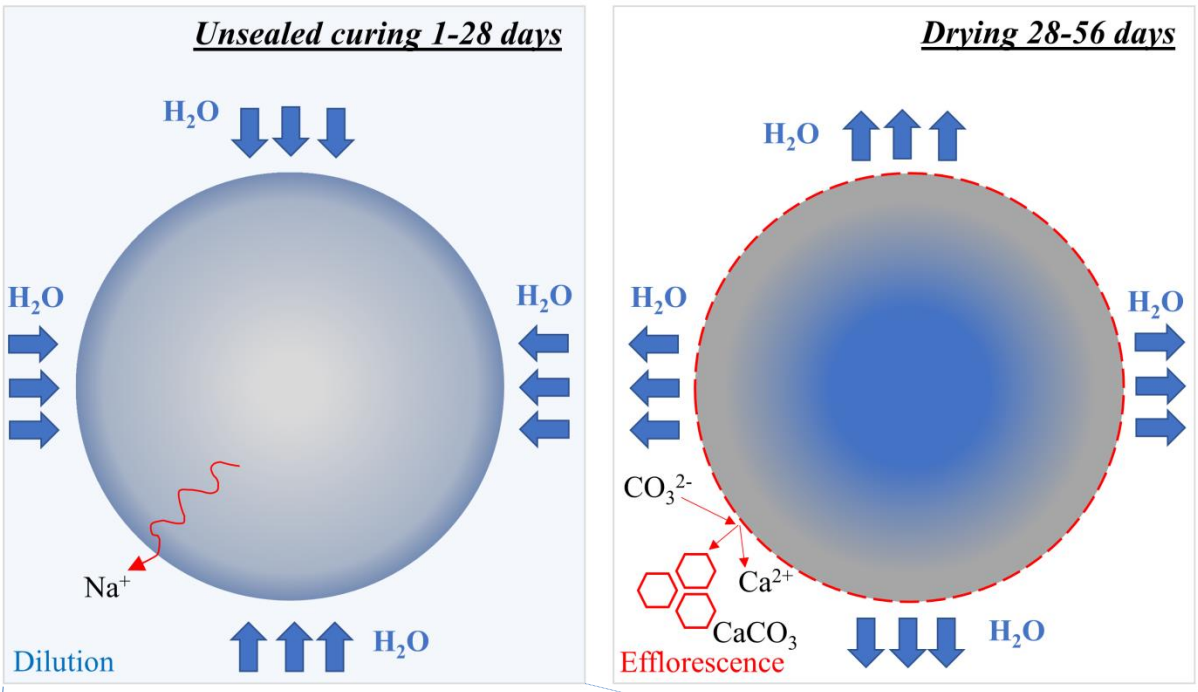

(a) Illustration of the direction of water transports during the unsealed curing (1-28 days) and drying of the pastes (28-56 days).

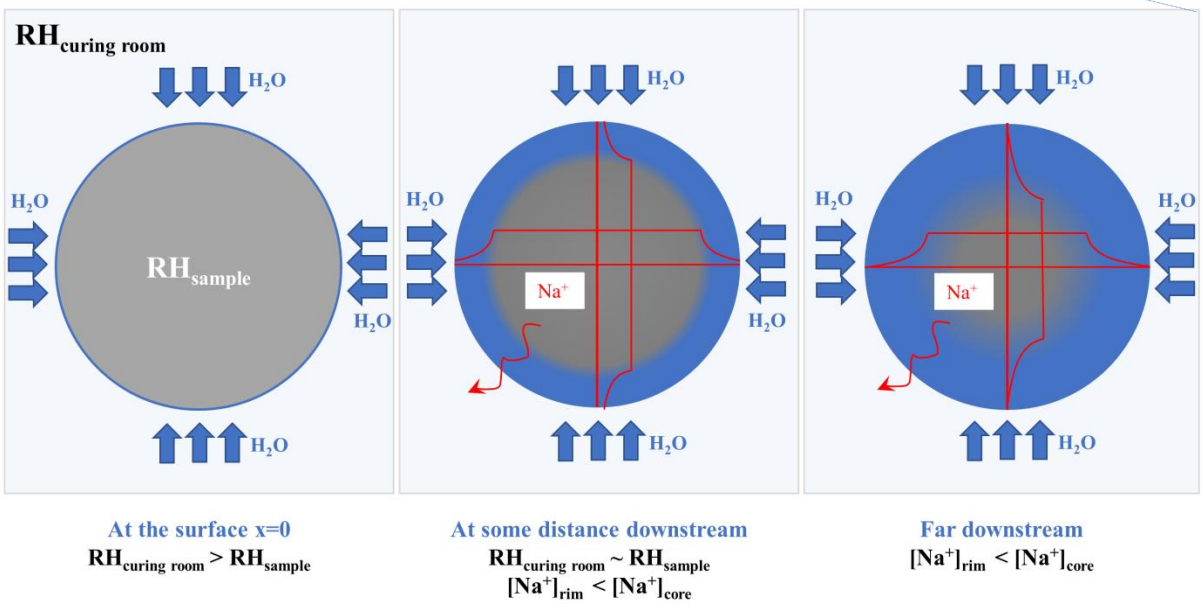

(b) Illustration of the boundary conditions during the water transport and Na^+ loss in the unsealed curing conditions of the pastes (1-28 days):
left: day 1, demoulding of the samples and subsequent exposure of the samples to 99% RH;
middle: advective movement of Na^+ by dilution of the pore solution at the surface of the samples followed by diffusive movement of Na^+;
right: diffusive movement of Na^+ from the interior towards the surface of the samples.

Fig. 5. (a) Illustration of the water transport during the unsealed curing (1-28 days) and drying of the pastes (28-56 days); (b) illustration of the boundary conditions during the water transfer and Na^+ loss in the unsealed curing conditions of the pastes (1-28 days).

The internal RH of the pastes was also measured at the age of 28 days (before storage in the laboratory conditions) and at the age of 56 days (after 28 days of storage in the laboratory conditions) as shown in Table 3. The RH of the unsealed samples is generally higher than the equivalent sealed samples, which is consistent with the pore fluids being more diluted in the unsealed samples, thus having a higher water activity. The results, presented in Table 3, show that the internal RH of the pastes at 28 days decreases with increment of GBFS content (from paste S0 to S100). This phenomenon can be attributed to the self-desiccation in these mixtures [34] and it has a similar effect on the sealed and unsealed samples.

The RH of the samples after 56 days shows that the samples have not reached the equilibrium condition with the environment yet. The internal RH of alkali-activated pastes is around 62-65% RH at this age. As the accelerated carbonation tests are performed at 60% RH, it is expected that RH of the samples was likely equilibrated with RH of exposure site in a short time after the start of the experiment. The pastes CEM I and CEM III/B showed a higher internal RH compared to alkali-activated pastes showing that the drying is slower in these materials. The internal RH of CEM I paste with water-to-cement ratio 0.5 at 28 days is in agreement with the literature [35].

3.1.2 pH and composition of the pore solution

The pore solution analysis was performed on both groups (sealed and unsealed) of samples after 28 and 56 days of curing. This analysis enabled the quantification of the concentration of the main ions (Na^+, K^+, Ca^{2+}, S^{2-}) in the pore solution and measurement of pH. Results of pH and composition of the pore solution are presented in Table 4 and Table 5.

Table 4

pH values and main element composition of pastes pore solutions analyzed with ICP-OES (28 days).The pore solutions were extracted with high pressure method.

		pH	[Na]	[K]	[Ca]	[S]	Porosity
Curing room (99% RH)		[-]	[mmol/L]	[mmol/L]	[mmol/L]	[mmol/L]	[%][36]
S0	Sealed	13.40	1336	20	21.73	298	
	Unsealed	13.02	101	4	33.08	< 1.5	43.71
S30	Sealed	13.45	1004	23	19.40	375	
	Unsealed	13.16	150	3	8.63	51	26.04
S50	Sealed	13.70	1078	26	8.48	292	
	Unsealed	13.30	211	4	3.35	79	9.4
S70	Sealed	13.80	1115	27	23.10	378	
	Unsealed	13.40	326	7	10.23	172	6.54
S100	Sealed	14.00	1556	36	29.50	573	
	Unsealed	13.60	551	11	19.63	326	3.57
CEM III B	Sealed	13.08	61	58	44.08	-	
	Unsealed	13.00	56	45	12.80	5	48.87
CEM I	Sealed	13.62	193	230	39.28	-	
	Unsealed	13.28	105	85	4.75	< 1.5	46.48

Table 5

pH values and main element composition of pastes pore solutions analyzed with ICP-OES (56 days). The pore solutions were extracted with high pressure method.

		pH	[Na]	[K]	[Ca]	[S]
		[-]	[mmol/L]	[mmol/L]	[mmol/L]	[mmol/L]
S0	Sealed*					
	Unsealed L**					
	Unsealed C***	12.40	29	1	3.80	
S30	Sealed*					
	Unsealed L**					
	Unsealed C***	13.00	106	2	3.15	
S50	Sealed*	13.72	1233	18	10.85	
	Unsealed L**	13.58	424	6	54.68	
	Unsealed C***	13.25	187	4	3.45	
S70	Sealed*	13.80	1363	32	29.55	0.42
	Unsealed L**	13.60	426	6	3.50	0.26
	Unsealed C***	13.34	268	6	5.58	
S100	Sealed*	14.00	1544	36	5.73	0.55
	Unsealed L**	13.60	557	10	12.88	0.32
	Unsealed C***	13.53	463	10	2.65	
CEM III	Sealed*					

B	Unsealed L**					
	Unsealed C***	13.05	59	53	1.95	
CEM I	Sealed*					
	Unsealed L**					
	Unsealed C***	13.29	116.13	79	15.58	

*Samples that were sealed cured for 28 days, demoulded at 28 days and further kept in unsealed laboratory conditions (55 % RH) until 56 days.

**Samples that were unsealed cured for 28 days, and further kept in unsealed laboratory conditions (55 % RH) until 56 days.

***Samples that were unsealed cured for 28 days, and further kept in unsealed curing conditions (99 % RH) until 56 days.

It can be observed that the pH of all sealed alkali-activated pastes is in the range of 13.4 to 14.0 at 28 days of curing, as expected. This value is lower in the unsealed equivalent pastes (but still higher than 13.0), which is due to Na-hydroxide loss from these specimens. Additionally, no specific change of pH is observed at 56 days of curing compared to 28 days (Fig. 6). A similar effect is also observed in CEM I paste. The pH in the sealed samples is generally higher than in unsealed pastes. This difference is smaller in CEM III/B pastes.

The $[Na^+]$ in the alkaline activator before mixing with raw materials was 4026 mmol/L. After 28 days of curing in sealed conditions, it can be seen that this value, in pastes (S0-S100), is reduced to the range of 1004 mmol/L to 1556 mmol/L (Fig. 7 left). It is clear that a part of Na^+ is taken up during the formation of reaction products, while the other part of Na^+ is present in the pore solution (or leached in the unsealed cured samples).

The effect of FA/GBFS ratio on the $[Na^+]$ in the pore solution is not clear at 28 days. The pastes S0 (100% FA) and S100 (100% GBFS) have the highest $[Na^+]$, while in pastes S30, S50 and S70 the $[Na^+]$ increases with increasing the content of GBFS. On the other hand, the $[K^+]$ always increases with increasing GBFS content (see Table 4). A relatively high $[S^{2-}]$ is found in the pore solutions with no specific correlation with the FA/GBFS ratio. Compared to pastes CEM I and CEM III/B, the pore solution in alkali-activated pastes contains a significantly higher $[Na^+]$, but a comparable $[K^+]$.

In contrast to CEM I and CEM III/B pastes, the [Na^+] of pore solutions of unsealed alkali activated pastes is still decreasing in all the pastes until 56 days in the curing room (Table 5). This decrease is higher in pastes with a higher percentage of FA (S0>S30>S50>S70>S100). This is in accordance with the differences in porosity of these specimens measured at 28 days with mercury intrusion porosimetry (Table 4). It can be also observed that the [Na^+] of the pore solutions of unsealed samples in laboratory conditions is higher than in the unsealed samples in curing room (see Fig. 7b). This was expected, as the high relative humidity in the curing room promotes the loss of Na^+ in these specimens.

A comparison between [Na^+], [K^+], [Ca^{2+}] and [S^{2-}] in all samples clearly shows a significant effect of the sealed and unsealed curing on the pore solution chemistry. A significant drop in ion concentration can be observed in the pore solution in the unsealed pastes. Fig. 7 shows the difference between [Na^+] in these specimens at 28 days and 56 days, respectively. It can be seen that these values are significantly lower in unsealed alkali-activated pastes, but still remain at a higher level compared to CEM I and CEM III/B pastes. The effect of loss on the [Na^+] in OPC-based pastes is also significant, but seems negligible in CEM III/B pastes. Alkali activated pastes, in direct contact with water during unsealed curing, show Na^+ leaching. There is, therefore, a competition between the Na^+ consumption for the reaction of FA and GBFS and the Na^+ loss due to leaching.

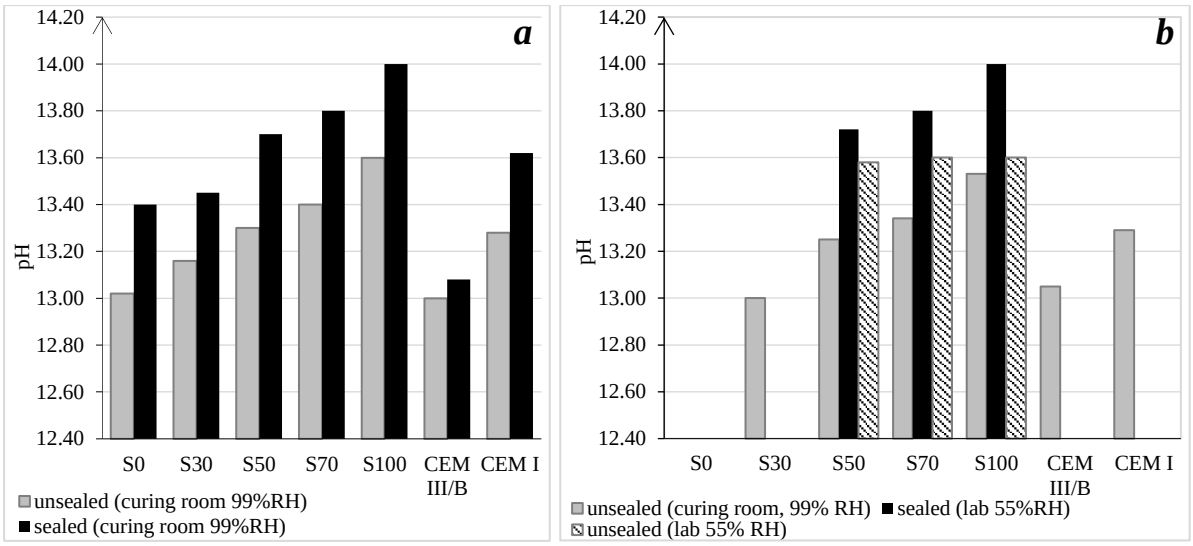

411

412 **Fig. 6.** The effect of sealing on the pH in the pore solution of the pastes at 28 days (a) and 56
413 days (b).

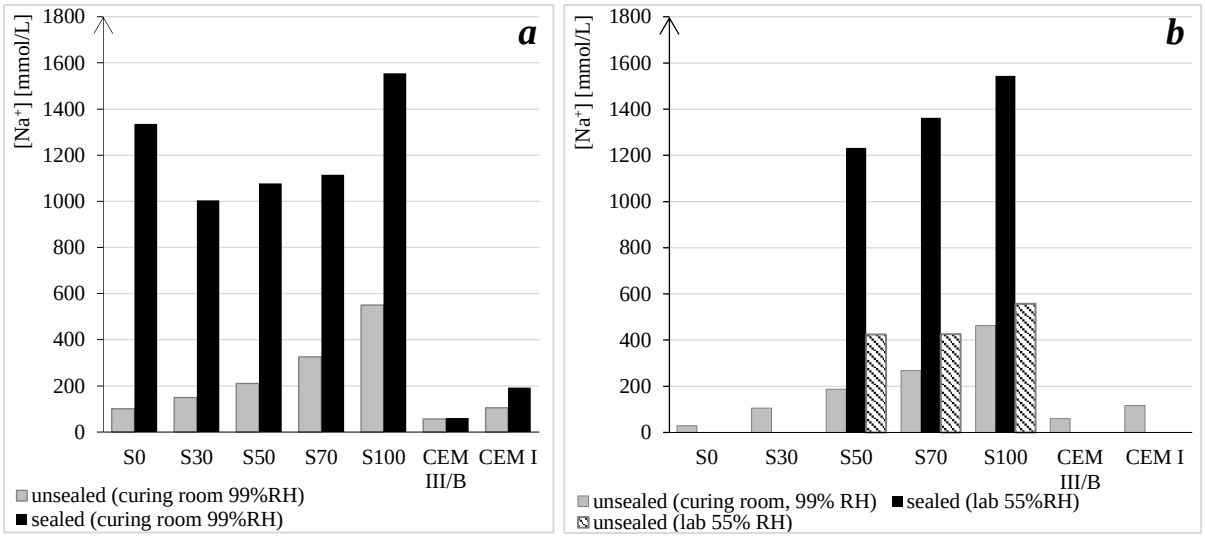

414

415 **Fig. 7.** The effect of sealing on the [Na^+] in the pore solution of the pastes at 28 days (a) and
416 56 days (b).

417

418 3.1.3 Alkali loss

419 The alkali content in the pore solution can vary depending on the type of the curing
420 conditions as shown in Section 3.1.2. Significant alkali loss was observed for unsealed cured
421 samples. The mechanism for alkali loss was explained in Section 3.1.1. The main role of the
422 alkalis is to provide the right environment for dissolution of the FA and GBFS. In addition,
423 the alkalis content in the pore solution of AAMs is highly important as they are the main

buffer for alkalinity during carbonation. Beside alkalis (Na), calcium ions may also contribute to maintaining a high pH of the pore solution. This is supported by the authors' previous study [37], where it was shown that not all the CaO was consumed by carbonation of studied alkali activated pastes. This implies that, after NaOH carbonation, the remaining CaO can act as a buffering agent for the pH of the pore solution.

Beside alkali loss, the efflorescence occurred in all samples cured in unsealed conditions, except for pastes CEM I, CEM III/B and S0 as was observed when they were moved from the fog room to the laboratory environment (55-60% RH). Although soluble silicate and GBFS addition are found beneficial in reducing the efflorescence degree in AAMs, they have limited influence on the overall efflorescence potential, as they appear to have a delaying rather than mitigating effect [38]. The coexistence of water with water-soluble salts and exposure to moisture gradients or wet/dry cycles are main conditions for efflorescence. Evaporation of the aqueous salt solution may occur on the surface or in regions near the surface when a moisture gradient between the ambient atmosphere and the material exists. This resulted in the appearance of efflorescence on the surface of the unsealed cured specimens (Fig. 8a). The efflorescence powder was collected carefully from the sample's surfaces for further chemical analysis (Fig. 8a).

SEM-EDX analysis showed that the product of efflorescence was calcite ($CaCO_3$), with the size of about 10-20 µm (Fig. 8b). Similar morphology was also observed in the study by García-Carmona et al. [39], where the calcite particles were obtained by carbonation of slaked lime in a semicontinuous process. The $CaCO_3$ formation in this study resulted from $Ca^{2+}OH^-$ carbonation when the CO_2 and H_2O are simultaneously present and when the solubility of calcite is exceeded. The $Ca^{2+}OH^-$ ion pair from solution is transported towards the surface of the hardened paste where it reacts away to carbonate at the cylinder surface (see Fig. 5). Since the precipitation takes Ca^{2+} out of solution, it is replenished by diffusion

through the fluid and re-equilibration (Ca-release) from the gel.The final result of the several steps through which the carbonates are formed can be described by the following reaction similar to [40]:

$$CO_2(aq) + Ca^{2+}(aq) + 2OH^-(aq) \rightarrow CaCO_3(s) + H_2O \quad (1)$$

Meanwhile, the deposits from the plastic container in which the moisture from the surface of the specimen S100 was collected after 1 day of unsealed curing, were also analyzed. The carbon together with oxygen, sodium, calcium and traces of aluminium, silicon, sulfur and potassium were detected as demonstrated by the EDX spectrum (Fig. 8c). The anhedral crystals (Fig. 8c) are identified as gaylussite ($Na_2Ca(CO_3)_2 \cdot 5H_2O$) because they are formed mostly of Na and Ca (EDX spectrum, Fig. 8c), similar to the gaylussite identification by Jones et al. [41]. The mechanism of the Na, Ca-carbonate formation can be described by the following reactions:

$$CO_2(g) + 2OH^-(aq) \rightarrow CO_3^{2-}(aq) + H_2O \quad (2)$$

$$2CO_3^{2-}(aq) + 2Na^+(aq) + Ca^{2+}(aq) + 5H_2O \rightarrow Na_2Ca(CO_3)_2 \cdot 5H_2O \quad (3)$$

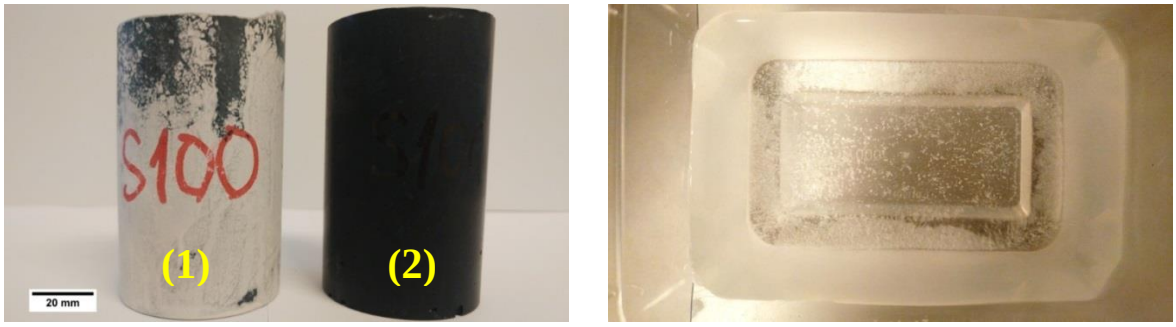

Fig. 8a. Pastes S100 at 56 days (left, (1)-unsealed cured sample, (2)-sealed cured sample), the plastic container in which the fluid, condensed on the surface of the specimen S100, was collected after 4 days of unsealed curing (right).

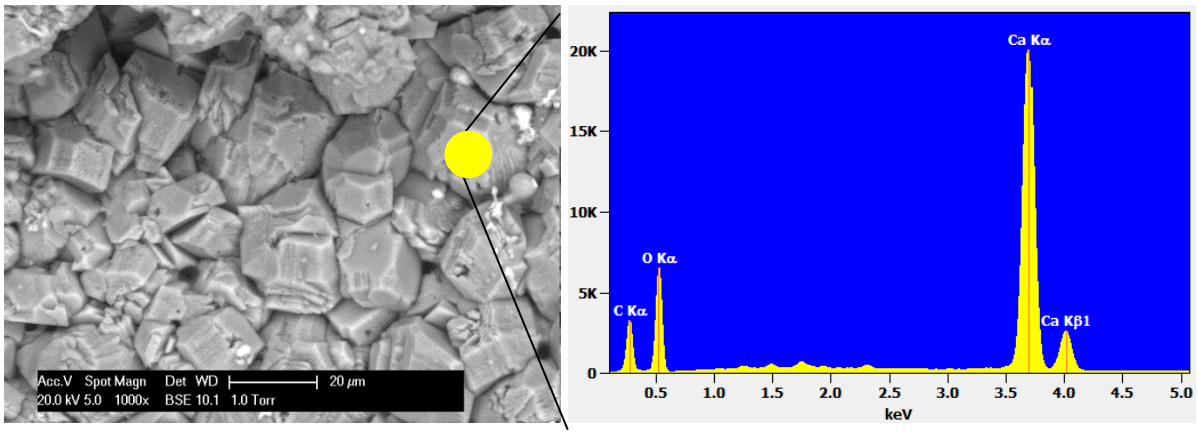

Fig. 8b. ESEM-BSE image and EDX spectrum of the deposit from the surface of the cylindric sample labelled as (1) shown in Fig. 8a.

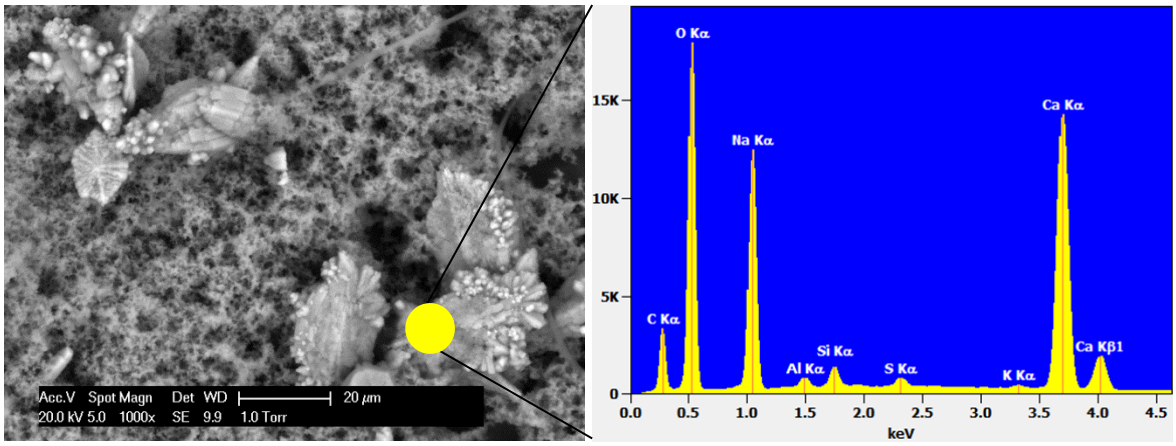

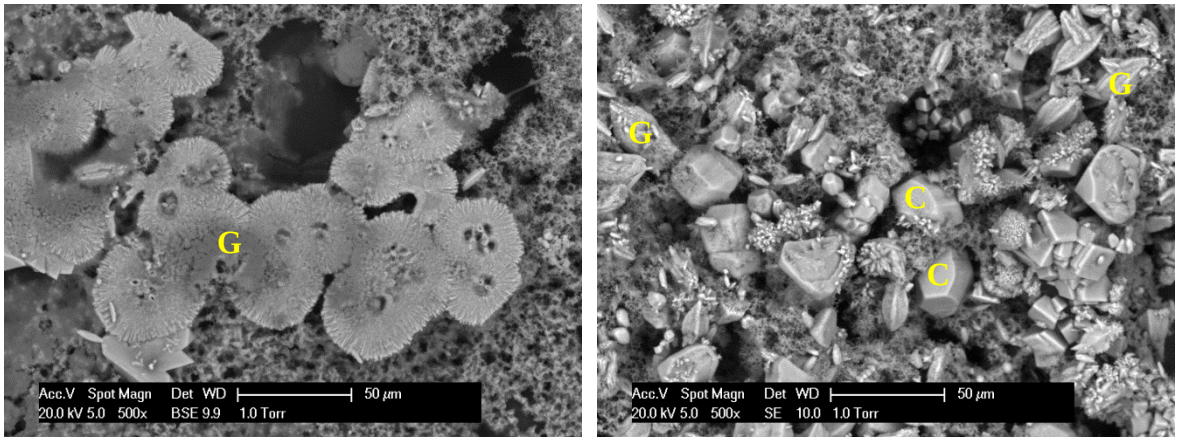

Fig. 8c. ESEM-BSE images and EDX spectrum of the deposit from the plastic container shown in Fig. 8a (Gaylussite-G, Calcite-C).

476 The ICP-OES results for Na^+ from alkali loss experiments of the pastes S50 and S100
477 are presented in Fig. 9. It should be noted that this figure shows the cumulative amount of the
478 Na^+ in the solutions collected in the plastic containers and for each stage the new measured
479 absolute amount of Na was added to the previous. The containers were removed for the Na^+
480 measurement and a new empty container was placed for the collection of the fluid in the next
481 time segment to avoid saturation of the solutions with the solids precipitating in the containers
482 as shown in Fig. 8a, c. The results clearly show the continuous loss of Na^+ from the samples
483 with time. It seems that the highest amount of alkali loss occurred between 7 and 28 days. The
484 leached Na amount is lower in specimen with higher GBFS content (Fig. 9). The higher alkali
485 loss in pastes S50 compared to pastes S100, is due to a more porous microstructure of paste
486 S50 compared to paste S100 as shown in Table 4, column 7. This facilitates the Na-leaching
487 process. Water from the curing atmosphere can more readily enter the gel and become self-
488 expelled in paste S50 compared to paste S100. The absolute mass of leached Na^+ was
489 measured from the total solution volume which was collected in the plastic container during
490 28 days of unsealed curing of the samples S50 and S100. It is found that 0.8 g and 0.65 g of
491 Na^+ was leached from the samples S50 and S100, respectively. The absolute amount of Na
492 which was initially used for the activation was 4.62 g. This implies that 17.3 % and 14 % of
493 this initial Na amount, was leached from the samples S50 and S100, respectively.

494 It should be noted that the ICP-OES analysis enabled the quantification of $[Na^+]$ in
495 solution but not of the $[Na^+]$ which already reacted with carbonate ions forming a solid during
496 alkali loss as found from SEM-EDX analysis (Fig. 8c). This implies that a higher amount of
497 Na was expelled than was measured in the experiments.

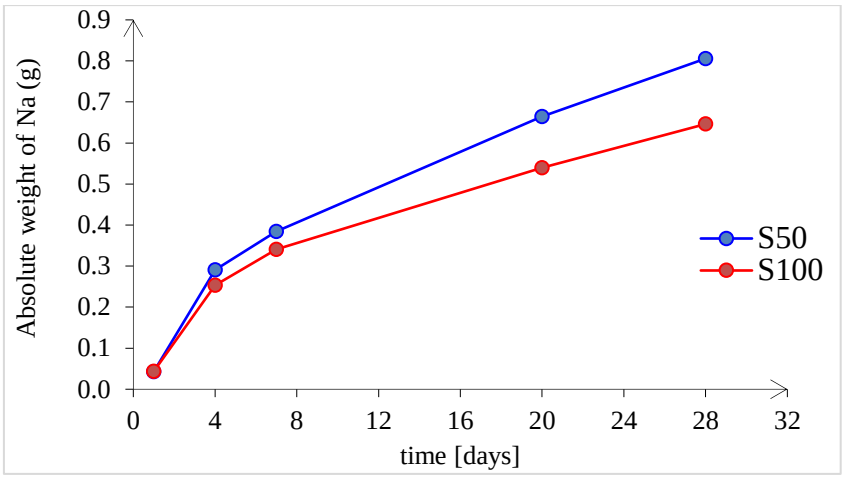

Fig. 9. Cumulative Na leached from the unsealed pastes (S50 and S100) during 28 days of curing in 99% RH.

3.2 Effect of accelerated carbonation

3.2.1 Carbonation depth

The carbonation depths were measured for both sealed and unsealed cured samples and the results are presented in Fig. 10.

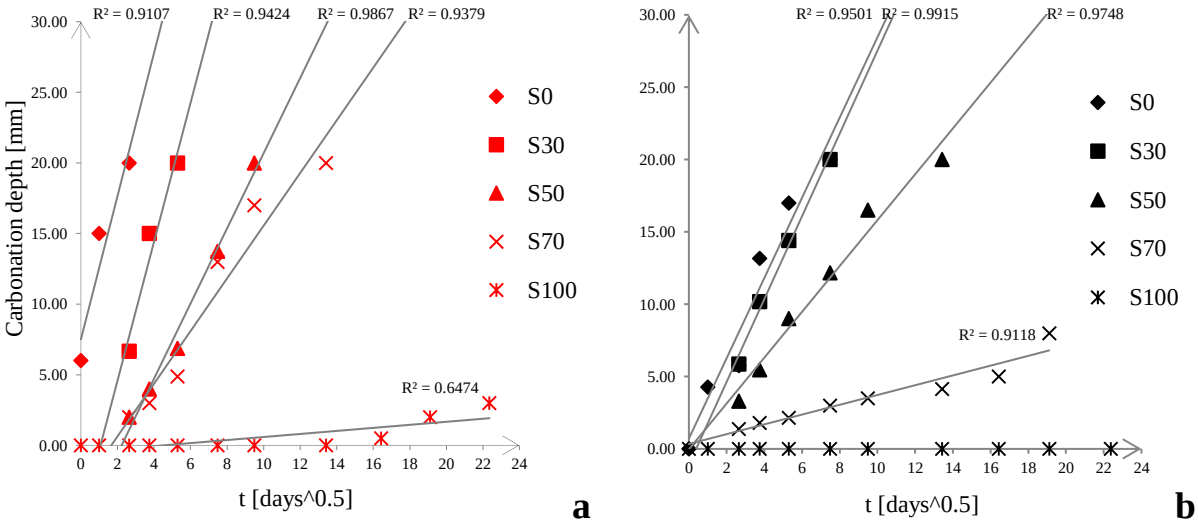

Fig. 10. Carbonation rate for the unsealed cured samples (a), and for the sealed cured samples (b). R^2 is the correlation coefficient from the least-squares linear fits.

Carbonation was observed in the pastes S0, S30, S50 even after 1 day of exposure. It can be seen that in general, the propagation rate of carbonation front is faster in the unsealed cured samples. The reason is that Na^+ leaching in unsealed samples leads to modification of the microstructure, composition of reaction products and the degree of reaction (compared to sealed cured samples), all of which have a strong influence on the carbonation resistance. These are indirectly supported by the previous study of the authors where it was shown that paste S100 has a different compressive strength development in sealed and unsealed curing conditions [42].

It can also be observed that, in unsealed samples, carbonation depth lines do not pass through the origin. While a positive intercept as a result of early carbonation of the paste during curing and preconditioning period can be observed in the paste S0, the other pastes show delayed carbonation. The latest is related to the paste S100 in which the carbonation was only detected after t=180 days of exposure. On the other hand, in sealed samples, all the curves pass through the origin besides the paste S100 in which carbonation was not observed. It can also be seen that the propagation rate of carbonation front (slope of the curves) significantly decreased with increasing GBFS content.

The carbonation depth seems to be linearly proportional to the square root of time (Fig. 10), that is similar to cement-based materials [43]. This relation is usually described by the Fick's 1^{st} law, whereas the slope of these curves corresponds to the diffusivity constant or carbonation coefficient K ($x=K\cdot t^{0.5}$, where x, carbonation depth; t, time in days).

The role of curing conditions in relation to GBFS content on carbonation coefficients is clear in Fig. 11. It seems that there is a certain threshold of GBFS content, after which the curing conditions affect the carbonation rate. This reflects the importance of calcium and

shows when the system is rich in GBFS, alkalis play a less important role in carbonation resistance of the samples in the studied carbonation conditions.

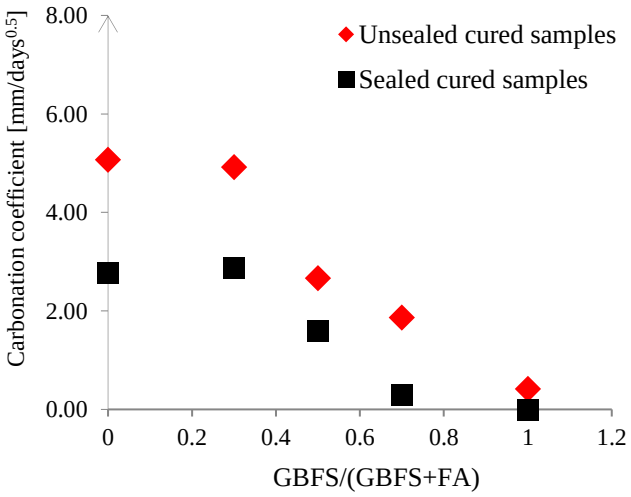

Fig. 11. The relationship between carbonation coefficients (K) and GBFS content for the unsealed cured samples and for the sealed cured samples. The carbonation coefficients are calculated using the data in Fig. 10, from linear fits of the carbonation depths as a function of the square root of time ($x=K\cdot t^{0.5}$).

3.2.2 pH of the pore solution

The pH of the simulated pore solution of the 500 days sealed cured reference and 500 days carbonated samples are presented in Fig. 12.

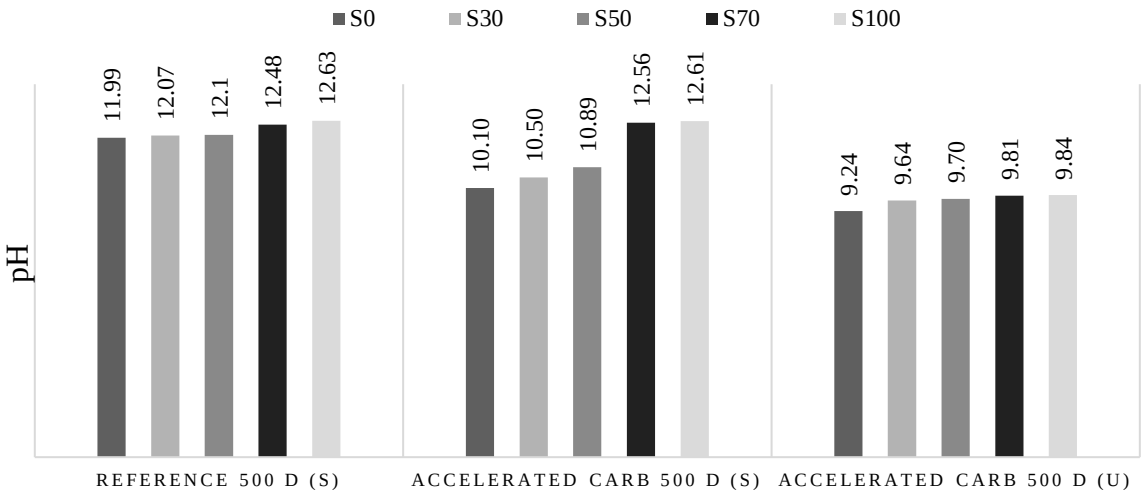

Fig. 12. pH of simulated pore solutions of alkali-activated pastes as a function of GBFS content in the paste and curing conditions (500 days cured reference (noncarbonated) pastes and 500 days under accelerated carbonation, S: sealed samples and U: unsealed samples cured for 28 days at curing conditions (20 ºC, ~99% RH) before their preconditioning and exposure to accelerated carbonation).

At a first glance, it is clear that the pH of the noncarbonated sealed cured pastes decreased from 13.40 ~ 14.00 at 28 days (see Table 4) to 11.99 ~ 12.63 at 500 days (see Fig. 12). This reduction can be attributed to the consumption of Na^+ and OH^- with the continuous hydration of the gel, as schematically presented in Fig. 13. A major part of Na^+ and OH^- is consumed for breaking up the alumino-silicate network of the FA glass (during hydration). In contrast, breaking up the GBFS network requires lower amount of alkalis. For this reason, the reduction of pH is higher in FA-rich pastes compared to GFBS-rich pastes. This is in accordance with a previous study [44] where it was shown that the uptake of Na^+ by the gel phases increases as the Ca/Si ratio decreases. This also implies that a higher [Na^+] is expected to be present in the pore solution of GBFS-rich pastes compared to FA-rich pastes prepared with the same initial amount of alkaline activator (S30<S50<S70<S100), see Table 4. A similar change of pH after 1 year of sealed curing was also reported by Pouhet and Cyr [45]

for alkali activated metakaoline and by Zuo et al. [46] for alkali activated GBFS. As schematically shown in Fig. 13, a larger reduction of pH is expected in the unsealed cured samples due to the leaching of Na^+ from the pore solution. In contrast, the pH buffering agent in cement-based materials (that is calcium from $Ca(OH)_2$ and C-S-H) increases until reaching the maximum degree of hydration and then it remains constant through the time. This ensures a longer passivation of the reinforcing steel surface when carbonation initiates in cement-based materials [47] compared to alkali activated pastes.

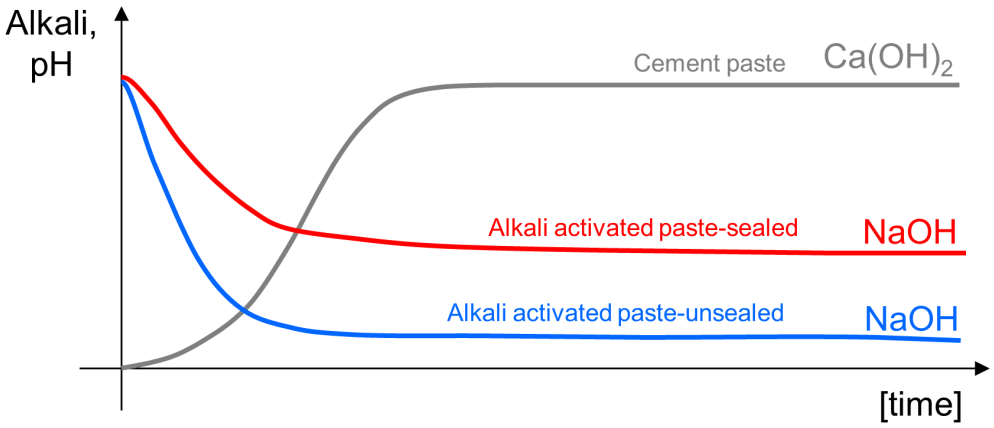

Fig. 13. Schematic illustration of the content of alkali sources in cement paste (grey line, alkali source: $Ca(OH)_2$) versus alkali activated paste, sealed (red line, alkali source: NaOH) and unsealed cured (blue line, alkali source: NaOH) during the hydration process.

In carbonated sealed cured alkali activated pastes, a clear reduction of pH is observed in S0, S30 and S50 samples (for example this value is reduced from 11.99 to 10.10 in paste S0). Meanwhile, the change of pH is negligible in the pastes with high GBFS contents (S70 and S100). In S100, this was expected because the paste was not carbonated. In paste S70, however, a reduction of pH was expected. As the carbonation occurred only in the microcracks of the sample S70, the carbonation front was not uniform and thin. The taken

powders were, therefore, a mix of carbonated and noncarbonated parts that led to a high pH. The role of Na^+ consumption is also insignificant in this paste due to the small portion of FA.

In unsealed samples, the reduction of pH after carbonation is much more than of the sealed cured samples. The pH of carbonated unsealed pastes, reaches a value of 9.24 in S0 and a value of 9.84 in S100. Note that all these pH values are related to the strongly carbonated outer surface material (for pastes S0, S30 and S50). This larger pH reduction is the result of three concurrent mechanisms: continuous FA and GBFS dissolution, Na^+ leaching, and carbonation of NaOH in the pore solution. Carbonation of NaOH is followed by dissolution of the calcium from the C-N-A-S-H gel which acts as a pH buffering agent. In samples with lower GBFS content, the amount of available calcium is less and thus the buffering capacity is less. Therefore, the pH of these samples after carbonation shows a larger reduction. It is assumed that a combination of $CaCO_3$ and gel phases with remaining Na^+ buffers the alkalinity above pH 9 for the GBFS containing pastes. On the other hand, it is likely that the NASH gel and remaining Na^+ buffer the alkalinity for carbonated paste S0. The obtained pH values in all carbonated unsealed cured samples are lower than the predicted pH values of Bernal et al. [19] for the same NaOH content and CO_2 concentration.

It is clear that the pH reduction occurs faster in carbonated alkali activated pastes compared to cement-based pastes. The combination of a low [Na^+] with an eventual Na^+ loss in unsealed curing conditions, leads to a lower pH. This could accelerate corrosion of reinforcing steel in carbonated samples unless the concentration of alkalis in the pore solution remains high at both early and later ages. This latter can be achieved when appropriate curing conditions are followed and the permeability of the material is sufficiently low. The obtained pH values in carbonated unsealed samples (see Fig. 12) are significantly low and near the limit of depassivation of the steel [1]. It should, however, be noted that these results are

obtained from alkali activated *pastes*. The effect of carbonation on the pore solution of alkali activated *concrete* needs further study.

4. Conclusions

The effect of curing conditions and GBFS content on the pore solution composition and carbonation resistance of the alkali-activated FA/GBFS pastes was investigated in this study. From the experimental observations, the following conclusions can be drawn:

- An alkali leaching mechanism was observed in the unsealed cured specimens. This is most likely the result of several counter-affecting mechanisms. The RH difference between the environment and the specimen, causes a capillary flow from the surface to the interior of the samples and, therefore, an inward movement of the ions (advection). Meanwhile, condensation of water on the surface of the samples leads to dilution of the ions at the surface compared to the interior of the specimens. This causes a diffusive movement of ions from the interior towards the surface of the samples. Here, the diffusive outward movement of ions governed the inward advective water movement that in total led to a loss of the alkali from the pore solution.
- A higher reduction of alkalinity was seen in pastes containing 0, 30, 50 wt.% GBFS in comparison to pastes containing 70 and 100 wt.% GBFS. The main reason is larger consumption of Na^+ and OH^- during FA dissolution in pastes containing a large content of FA. The binding of Na^+ by the gel phases of the alkali activated paste reduces the effective $[Na^+]$ in the pore solution and hence the alkalinity of the pore solution. The GBFS-rich pastes have a lower Na^+-binding capacity, hence there is a higher $[Na^+]$ in the pore solution. This ensures a larger alkalinity buffer of the pore solution once the carbonation occurs in GBFS-rich pastes.

- Alkali leaching led to a faster propagation rate of carbonation front in unsealed samples. The replacement of FA by GBFS significantly improved the carbonation resistance independent from the curing condition.
- Based on the results for evolution of pH and propagation rate of carbonation, there are two reasons of pH decrease at long-term:
  - the pH of alkali activated pastes decreased due to ongoing gel formation (from pH 13.40 – 14.00 after 28 days of sealed curing to the pH 11.99-12.63 after 500 days (see Fig. 12)).
  - the pH decreased due to neutralization of the alkalis in the pore solution of the pastes under carbonation.

  As can be seen, curing may affect the long-term performance of AAMs not only in view of carbonation, but also in view of gel formation at later ages. The availability of alkalis is a first preventive measure for obtaining satisfactory carbonation resistance of AAMs.
- Since carbonation of AAMs is of a major practical interest, the results presented here show that sealed curing conditions certainly contribute to the production of more durable alkali-activated FA/GBFS materials against carbonation. This is in contrast to the traditional curing of OPC-based concretes, where the curing under water of OPC-based concretes favours the cement hydration, especially in the external layer of the OPC-based concrete specimens.

Acknowledgement

This research was carried out under the project S81.1.13498 in the framework of the Partnership Program of the Materials innovation institute M2i (www.m2i.nl) and the Technology Foundation STW (www.stw.nl), which is part of the Netherlands Organisation for Scientific Research (www.nwo.nl). The first author thanks Rob Polder from Microlab, TU

Delft (the Netherlands) for valuable discussions. The second author acknowledges the financial support of the European Union's Marie Curie Individual Fellowship program under REAgrant agreement No. 701531. The authors also thank anonymous reviewers for their comments which substantially improved the quality of this paper.

References

[1] L. Bertolini, B. Elsener, P. Pedeferri, E. Redaelli, R.B. Polder, Carbonation-Induced Corrosion, in: Corrosion of Steel in Concrete: Prevention, Diagnosis, Repair, Second Edition, John Wiley & Sons, 2013, pp. 79-92.

[2] L.J. Parrott, Damage caused by carbonation of reinforced concrete, Mater. Struct. 23(3) (1990) 230-234.

[3] V.G. Papadakis, C.G. Vayenas, M.N. Fardis, Experimental investigation and mathematical modeling of the concrete carbonation problem, Chem. Eng. Sci. 46(5–6) (1991) 1333-1338.

[4] A.V. Saetta, B.A. Schrefler, R.V. Vitaliani, The carbonation of concrete and the mechanism of moisture, heat and carbon dioxide flow through porous materials, Cem. Concr. Res. 23(4) (1993) 761-772.

[5] M. Thiéry, G. Villain, P. Dangla, G. Platret, Investigation of the carbonation front shape on cementitious materials: Effects of the chemical kinetics, Cem. Concr. Res. 37(7) (2007) 1047-1058.

[6] A. Hidalgo, C. Domingo, C. Garcia, S. Petit, C. Andrade, C. Alonso, Microstructural changes induced in Portland cement-based materials due to natural and supercritical carbonation, J. Mater. Sci. 43(9) (2008) 3101-3111.

[7] K. Arbi, M. Nedeljković, Y. Zuo, G. Ye, A Review on the Durability of Alkali-Activated Fly Ash/Slag Systems: Advances, Issues, and Perspectives. Ind. Eng. Chem. Res. 55(19) (2016) 5439-5453.

[8] A. Morandeau, M. Thiéry, P. Dangla, Investigation of the carbonation mechanism of CH and C-S-H in terms of kinetics, microstructure changes and moisture properties, Cem. Concr. Res. 56(0) (2014) 153-170.

[9] A. Leemann, P. Nygaard, J.Kaufmann, R. Loser, Relation between carbonation resistance, mix design and exposure of mortar and concrete, Cem. Concr. Compos. 62 (2015) 33-43.

[10] Z. Shi, B. Lothenbach, M.R. Geiker, J. Kaufmann, A. Leemann, S. Ferreiro, J. Skibsted, Experimental studies and thermodynamic modeling of the carbonation of Portland cement, metakaolin and limestone mortars, Cem. Concr. Res. 88 (2016) 60-72.

[11] P.H. Borges, J.O. Costa, N.B. Milestone, C.J. Lynsdale, R.E. Streatfield, Carbonation of CH and C–S–H in composite cement pastes containing high amounts of BFS, Cem. Concr. Res. 40(2) (2010) 284-292.

[12] Y. Ma, G. Ye, J. Hu, Micro-mechanical properties of alkali-activated fly ash evaluated by nanoindentation, Constr. Build. Mater. 147 (2017) 407-416.

[13] C.E. White, L.L. Daemen, M. Hartl, K. Page, Intrinsic differences in atomic ordering of calcium (alumino) silicate hydrates in conventional and alkali-activated cements, Cem. Concr. Res. 67 (2015) 66-73.

[14] R.J. Myers, S.A. Bernal, R. San Nicolas, J.L. Provis, Generalized structural description of calcium–sodium aluminosilicate hydrate gels: the cross-linked substituted tobermorite model, Langmuir, 29(17) (2013) 5294-5306.

[15] M.B. Haha, B. Lothenbach, G. Le Saout, F. Winnefeld, Influence of slag chemistry on the hydration of alkali-activated blast-furnace slag - Part I: Effect of MgO, Cem. Concr. Res. 41(9) (2011) 955-963.

[16] M. Palacios, F. Puertas, Effect of Carbonation on Alkali-Activated Slag Paste, J. Am. Ceram. Soc. 89(10) (2006) 3211-3221.

[17] F. Puertas, M. Palacios, T. Vázquez, Carbonation process of alkali-activated slag mortars, J. Mater. Sci. 41(10) (2006) 3071-3082.

[18] S.A. Bernal, R.M. de Gutiérrez, A.L. Pedraza, J.L. Provis, E.D. Rodriguez, S. Delvasto, Effect of binder content on the performance of alkali-activated slag concretes, Cem. Concr. Res. 41(1) (2011) 1-8.

[19] S.A. Bernal, J.L. Provis, D.G. Brice, A. Kilcullen, P. Duxson, J.S. van Deventer, Accelerated carbonation testing of alkali-activated binders significantly underestimates service life: The role of pore solution chemistry, Cem. Concr. Res. 42(10) (2012) 1317-1326.

[20] S.A. Bernal, J.L. Provis, B. Walkley, R. San Nicolas, J.D. Gehman, D.G. Brice, A.R. Kilcullen, P. Duxson, J.S. van Deventer, Gel nanostructure in alkali-activated binders based on slag and fly ash, and effects of accelerated carbonation, Cem. Concr. Res. 53 (0) (2013) 127-144.

[21] S.A. Bernal, R. San Nicolas, R.J. Myers, R.M. de Gutiérrez, F. Puertas, J.S. van Deventer, J.L. Provis, MgO content of slag controls phase evolution and structural changes induced by accelerated carbonation in alkali-activated binders, Cem. Concr. Res. 5(0) (2014) 33-43.

[22] M. Nedeljković, B. Šavija, Y. Zuo, M. Luković, G. Ye, Effect of natural carbonation on the pore structure and elastic modulus of the alkali-activated fly ash and slag pastes. Constr. Build. Mater., 161 (2018) 687-704.

[23] N. Li, N. Farzadnia, C. Shi, Microstructural changes in alkali-activated slag mortars induced by accelerated carbonation, Cem. Concr. Res. 100 (2017) 214-226.

[24] S.A. Bernal, J.L. Provis, R.M. De Gutiérrez, J.S. van Deventer, Accelerated carbonation testing of alkali-activated slag/metakaolin blended concretes: effect of exposure conditions, Mater. Struct. (2014) 1-17.

[25] F.R. Škvára, V. Šmilauer, P.E. Hlaváček, L.U. Kopecký, Z. Cilova. A weak alkali bond in (N, K)–A–S–H gels: evidence from leaching and modeling, Ceram Silik, 56(4) (2012) 374-382.

[26] R.R. Lloyd, J.L. Provis, J.S.J. van Deventer, Pore solution composition and alkali diffusion in inorganic polymer cement, Cem. Concr. Res. 40(9) (2010) 1386-1392.

[27] N. Ukrainczyk, O. Vogt, E.A. Koenders, Reactive Transport Numerical Model for Durability of Geopolymer Materials, Advances in Chemical Engineering and Science, 6(04) (2016) 355.

[28] H. Huang, G. Ye, Examining the “time-zero” of autogenous shrinkage in high/ultra-high performance cement pastes, Cem. Concr. Res. 97 (2017) 107-114.

[29] J. Kempl, O. Çopuroğlu, EH-pH- and main element analyses of Blast Furnace Slag Cement paste pore solutions activated with sodium monofluorophosphate – Implications for carbonation and self-healing, Cem. Concr. Compos. 71 (2016) 63-76.

[30] M. Babaee, M.S.H. Khan, A. Castel, Passivity of embedded reinforcement in carbonated low-calcium fly ash-based geopolymer concrete. Cem. Concr. Compos. 85(Supplement C) (2018) 32-43.

[31] Y. Ma, J. Hu, G. Ye, The pore structure and permeability of alkali activated fly ash. Fuel 104 (2013) 771-780.

[32] M. Nedeljković, K. Arbi, Y. Zuo, G. Ye, Microstructural and mineralogical analysis of alkali activated fly ash-slag pastes. The 3rd International RILEM Conference on Microstructure Related Durability of Cementitious Materials (2016) Nanjing, China,

[33] C. Dow, F.P. Glasser, Calcium carbonate efflorescence on Portland cement and building materials. Cem. Concr. Res. 33(1) (2003) 147-154.

[34] Z. Li, M. Nedeljković, Y. Zuo, G. Ye, Autogenous shrinkage of alkali-activated slag – fly ash pastes, in 5th International Slag Valorisation Symposium (2017) Leuven, Belgium.

[35] Z. Jiang, Z. Sun, P. Wang, Internal relative humidity distribution in high-performance cement paste due to moisture diffusion and self-desiccation. Cem. Concr. Res. 36(2) (2006) 320-325.

[36] M. Nedeljković, K. Arbi, Y. Zuo, G. Ye, Physical properties and pore solution analysis of alkali-activated fly ash-slag pastes, International RILEM Conference Materials Systems and Structures in Civil Engineering (2016) Lyngby, Denmark.

[37] M. Nedeljković, K. Arbi, Y. Zuo, G. Ye, CO_2 binding capacity of alkali-activated fly ash and slag pastes. Ceram. Int. (2018)

[38] Z. Zhang, J.L. Provis, A. Reid, H. Wang, Fly ash-based geopolymers: The relationship between composition, pore structure and efflorescence, Cem. Concr. Res. 64(Supplement C) (2014) 30-41.

[39] J. García Carmona, J. Gómez Morales, R. Rodríguez Clemente, Rhombohedral–scalenohedral calcite transition produced by adjusting the solution electrical conductivity in the system $Ca(OH)_2$–CO_2–H_2O. J. Colloid Interface Sci. 261(2) (2003) 434-440.

[40] H.F. Taylor, Cement chemistry, second ed. Thomas Telford, 1997.

[41] J B. Jones, X. Peng, Hot spring deposits on a cliff face: A case study from Jifei, Yunnan Province, China, Sediment. Geol. 302 (2014) 1-28.

[42] M. Nedeljković, Y. Zuo, K. Arbi, G. Ye, Carbonation Resistance of Alkali-Activated Slag Under Natural and Accelerated Conditions. Journal of Sustainable Metallurgy, 4(1) (2018) 33-49.

[43] I.S. Yoon, O. Çopuroğlu, K.B. Park, Effect of global climatic change on carbonation progress of concrete, Atmos. Environ. 41(34) (2007) 7274-7285.

[44] R.J. Myers, J.L. Provis, B. Lothenbach, Composition–solubility–structure relationships in calcium (alkali) aluminosilicate hydrate (C-(N, K-)ASH), Dalton Trans. 44(30) (2015) 13530-13544.

[45] R. Pouhet, M. Cyr, Carbonation in the pore solution of metakaolin-based geopolymer. Cem. Concr. Res. 88 (2016) 227-235.

[46] Y. Zuo, M. Nedeljković, G. Ye, Coupled thermodynamic modelling and experimental study of sodium hydroxide activated slag. Constr. Build. Mater. 188 (2018) 262-279.

[47] J.H.M. Visser, Influence of the carbon dioxide concentration on the resistance to carbonation of concrete. Constr. Build. Mater. 67 (2014) 8-13.

List of figures:

812 Fig. 9. Cumulative Na leached from the unsealed pastes (S50 and S100) during 28 days of
813 curing in 99% RH.

814 Fig. 10. Carbonation rate for the unsealed cured samples (a), and for the sealed cured samples
815 (b).

816 Fig. 11. The relationship between carbonation coefficients (K) and GBFS content for the
817 unsealed cured samples, and for the sealed cured samples. The carbonation coefficients are
818 calculated using the data in Fig. 10, from linear fits of the carbonation depths as a function of
819 the square root of time ($x=K\cdot t^{0.5}$). R^2 is the correlation coefficient from the least-squares
820 linear fits.

821 Fig. 12. pH of simulated pore solutions of alkali-activated pastes as a function of GBFS
822 content in the paste and curing conditions (500 days cured reference (noncarbonated) pastes
823 and 500 days under accelerated carbonation, S: sealed samples and U: unsealed samples cured
824 for 28 days at curing conditions (20 ºC, ~99% RH) before their preconditioning and exposure
825 to accelerated carbonation).

826 Fig. 13. Schematic illustration of the content of alkali sources in cement paste (grey line,
827 alkali source: Ca(OH)2) versus alkali activated paste, sealed (red line, alkali source: NaOH)
828 and unsealed cured (blue line, alkali source: NaOH) during the hydration process.

829 List of tables:

830 Table 1
831 Chemical composition of FA, GBFS, CEM I (42.5 N), CEM III/B measured with XRF [%].
832 Table 2
833 Mixture design for pastes with respect to 100 g of binder.
834 Table 3
835 Water loss (in mass percentage) and internal RH of the pastes*.

836 Table 4

837 pH values and main element composition of pastes pore solutions analyzed with ICP-OES (28
838 days). The pore solutions were extracted with high pressure method.

839 Table 5

840 pH values and main element composition of pastes pore solutions analyzed with ICP-OES (56
841 days). The pore solutions were extracted with high pressure method.